# Pathways of Meltwater Export from Petermann Glacier, Greenland

CÉLINE HEUZÉ AND ANNA WÅHLIN

*Department of Marine Sciences, University of Gothenburg, Gothenburg, Sweden*

HELEN L. JOHNSON

*Department of Earth Sciences, University of Oxford, Oxford, United Kingdom*

ANDREAS MÜNCHOW

*College of Earth, Ocean, and Environment, University of Delaware, Newark, Delaware*

(Manuscript received 18 July 2016, in final form 5 December 2016)

ABSTRACT

Intrusions of Atlantic Water cause basal melting of Greenland's marine-terminating glaciers and ice shelves, such as that of Petermann Glacier, in northwest Greenland. The fate of the resulting glacial meltwater is largely unknown. It is investigated here, using hydrographic observations collected during a research cruise in Petermann Fjord and adjacent Nares Strait onboard icebreaker (I/B) *Oden* in August 2015. A three end-member mixing method provides the concentration of Petermann ice shelf meltwater. Meltwater from Petermann is found in all of the casts in adjacent Nares Strait, with the highest concentration along the Greenland coast in the direction of Kelvin wave phase propagation. The meltwater from Petermann mostly flows out on the northeast side of the fjord as a baroclinic boundary current, with the depth of maximum meltwater concentrations approximately 150 m and shoaling along its pathway. At the outer sill, which separates the fjord from the ambient ocean, approximately 0.3 mSv (1 Sv $\equiv 10^6\,m^3\,s^{-1}$) of basal meltwater leaves the fjord at depths between 100 and 300 m. The total geostrophic heat and freshwater fluxes close to the glacier's terminus in August 2015 were similar to those estimated in August 2009, before the two major calving events that reduced the length of Petermann's ice tongue by nearly a third and despite warmer inflowing Atlantic Water. These results provide a baseline but also highlight what is needed to assess properly the impact on ocean circulation and sea level of Greenland's mass loss as the Atlantic Water warms up.

## 1. Introduction

Greenland glaciers are melting, increasingly quickly, in response to climate change (e.g., Zwally et al. 2011; Khan et al. 2014; Velicogna et al. 2014). The resulting extra freshwater contributes to current sea level rise (Nick et al. 2013) and can potentially disturb the North Atlantic Ocean circulation (Swingedouw et al. 2009; Bamber et al. 2012). Yet, models cannot produce reliable sea level or circulation projections, for we know neither how much meltwater exits the Greenland fjords nor where it goes (Flato et al. 2013).

Greenland's marine-terminating glaciers are becoming thinner and retreating due to changes caused by the warming of both the atmosphere and the ocean (Straneo et al. 2013). Among marine-terminating glaciers, Petermann Glacier (PG) in northwest Greenland is one of the largest, with a floating ice tongue 48 km long, 17 km wide, and 200 m thick at the terminus (Münchow et al. 2014). PG recently lost approximately 20% of its ice tongue by calving in 2010 (Falkner et al. 2011) and 20% more in 2012 (Münchow et al. 2014). Although visually dramatic, calving may not be the largest contributor to Petermann's mass balance: observations suggest that up to 80% of its mass loss may be due to basal melting only (Rignot 1996; Nick et al. 2012; Enderlin and Howat 2013).

Past hydrographic campaigns have shown that modified Atlantic Water (AW) from Nares Strait (Münchow and Melling 2008) intrudes into the fjord (Johnson et al. 2011) and under the ice tongue (Rignot and Steffen 2008). Over the comparatively warm and salty Atlantic Water lies a cold and freshwater mass alternatively called Arctic Water (Aagaard et al. 1981), Polar Water (Straneo et al. 2012), or Winter Water (WW; Johnson et al. 2011). Both

*Corresponding author e-mail*: Céline Heuzé, celine.heuze@marine.gu.se

DOI: 10.1175/JPO-D-16-0161.1

© 2017 American Meteorological Society. For information regarding reuse of this content and general copyright information, consult the AMS Copyright Policy (http://www.ametsoc.org/PUBSCopyrightPolicy).

the modified Atlantic Water and the Winter Water have been advected from the Arctic (Coachman and Aagaard 1974) and into Petermann Fjord (Straneo et al. 2012). For a review of the properties of these water masses in the vicinity of Greenland's marine-terminating glaciers, the reader is referred to Straneo et al. (2012).

Remote sensing can provide estimates of how much meltwater is produced (Enderlin and Howat 2013); however, these observations do not map pathways of the glacial meltwaters. We here expand on the first oceanographic description of Petermann Fjord by Johnson et al. (2011) and provide a first assessment of the paths of its meltwater, inside and outside the fjord, based on the temperature and salinity data that we collected in August 2015 from icebreaker (I/B) *Oden*. To do so, we use methods developed for the study of Antarctic ice shelves, where similarly the intrusion of relatively warm circumpolar deep water under the ice causes melting. Gade (1979) showed that the temperature plotted as a function of the salinity of water resulting from the melting of an ice shelf would align along a specific line (the so-called Gade line); Jenkins (1999) extended the Gade (1979) analysis to include the interaction with a third water mass. Wåhlin et al. (2010) and others have subsequently used the Gade line to define the presence of meltwater in the water column.

The hydrographic data collected are detailed in section 2, along with our methods. We show where and how much meltwater from Petermann can be detected in our study area in section 3 and describe the circulation of this meltwater inside and outside the fjord in section 4. We conclude in section 5, after briefly comparing our results to those obtained by Johnson et al. (2011) based on data collected prior to Petermann's recent calving events.

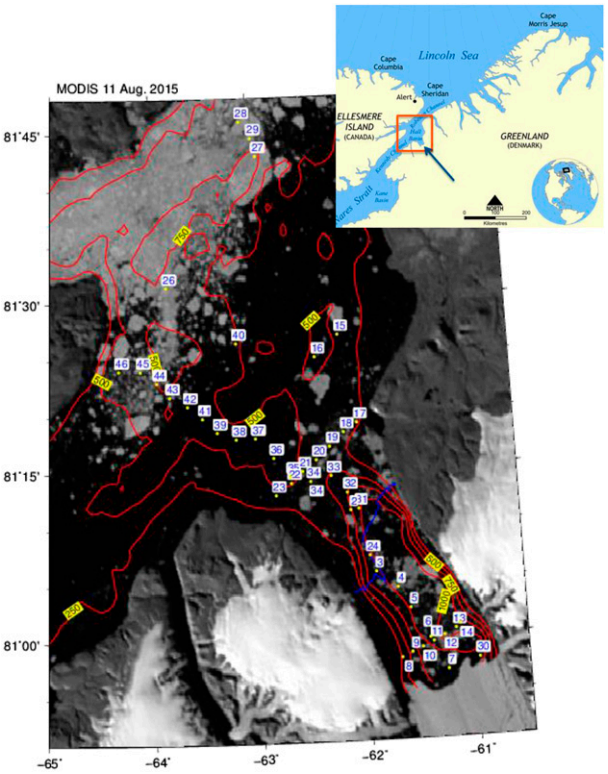


FIG. 1. Location of all the CTD casts of the Petermann2015 expedition, overlaying the MODIS–*Terra* reflectivity map from 11 Aug 2015. Red contours are 250-, 500-, 750-, and 1000-m isobaths obtained from the International Bathymetric Chart of the Arctic Ocean, version 3.0 (IBCAO-3), bottom topography (Jakobsson et al. 2012) augmented by 2009 and 2012 echo sounder surveys. The blue line indicates the location of the casts performed at the then terminus in 2009. In the top-right corner, see the Petermann Fjord in relation to the rest of the world; arrow indicates the glacier and red square is our 2015 study area (after Norman Einstein for Wikipedia Commons).

## 2. Data and methods

Figure 1 shows Petermann Fjord and adjacent Nares Strait in northwest Greenland at approximately 81°N and 60°W. The glacier itself is located in the southeast of our study area and flows into the fjord that is orientated southeast–northwest. The floating ice tongue is currently about 48 km long; for comparison, the location of the terminus in 2009 (Johnson et al. 2011) is indicated in blue in Fig. 1. Petermann Fjord is separated from Hall Basin by a 500-m-deep sill (Fig. 1, casts 17 to 23). Hall Basin is part of Nares Strait, which separates Greenland in the east from Canada's Ellesmere Island in the west and connects the Arctic Ocean in the north to Baffin Bay in the south.

The hydrographic measurements used in this study were collected in August 2015 on board the Swedish icebreaker *Oden* during the geological/glaciological Petermann 2015 expedition. Hydrographic data were sampled with an SBE911+ conductivity–temperature–depth (CTD) system from Sea-Bird Electronics, Inc. (SBE). The temperature, conductivity, and oxygen sensors were calibrated before and after the cruise. The CTD station positions are shown in Fig. 1. In situ conductivity and temperature have been converted to Conservative Temperature $\Theta$ (hereinafter referred to as temperature) and Absolute Salinity SA (hereinafter referred to as salinity) using the TEOS-10 equation of state (McDougall and Barker 2011). Oxygen concentration O2 was obtained only from cast 26 onward (after 20 August 2015). Assuming that the terminus, at the end of the 48-km-long ice tongue, is in hydrostatic balance, the ice draft at the terminus was approximated by multiplying by 9.34 the ice elevation data from NASA's operation IceBridge (Münchow et al. 2014).

For each cast, we assess the amount of meltwater produced from the melting of the Petermann ice shelf by

TABLE 1. Seawater properties used in the three water masses' mixture equation, range of these values in Petermann Fjord and Hall Basin, and corresponding potential temperature and practical salinity.

| Water mass | Θ (°C) | SA (g kg$^{-1}$) | O2 (ml l$^{-1}$) | Potential temperature (°C) | Practical salinity |
|---|---|---|---|---|---|
| Atlantic Water | 0.28 ± 0.02 | 34.93 ± 0.02 | 6.58 ± 0.01 | 0.29 ± 0.02 | 34.77 ± 0.02 |
| Petermann Glacier Water | −91.45 ± 0.14 | 0.00 | 27.00 ± 0.50 | −93.04 ± 0.04 | 0.00 |
| Winter Water | −1.78 ± 0.09 | 30.78 ± 0.40 | 7.62 ± 0.15 | −1.79 ± 0.08 | 30.63 ± 0.40 |

the underlying Atlantic Water using the three water mass mixture equation of Jenkins (1999). This calculation deduces the glacial meltwater concentration arising due to the melt of an ice shelf into a stratified water column. It considers the effect of mixing between three different water masses on conservative properties of the mixture (here temperature, salinity, and oxygen concentration). The three water masses involved in this calculation are the Atlantic Water (Θ = 0.28°C, SA = 34.93 g kg$^{-1}$, and O2 = 6.58 ml l$^{-1}$; see Table 1), the cold and fresh water overlying AW that we refer to as Winter Water (Θ = −1.78°C, SA = 30.78 g kg$^{-1}$, and O2 = 7.62 ml l$^{-1}$) for consistency with Johnson et al. (2011) and the Antarctic studies where this method has previously been used (e.g., Jenkins 1999; Wåhlin et al. 2010; Jacobs et al. 2011), and the effective properties of PG, which we refer to as Petermann Glacier Water (PGW; Θ = −91.45°C, SA = 0 g kg$^{-1}$, and O2 = 27 ml l$^{-1}$).

For a water mass with hydrographic properties SA and Θ, the concentration of melted ice shelf water is given by

$$\text{meltwater content} = \frac{\Theta - \Theta_{AW} - \dfrac{(SA - SA_{AW})(\Theta_{WW} - \Theta_{AW})}{SA_{WW} - SA_{AW}}}{\Theta_{PGW} - \Theta_{AW} - \dfrac{(SA_{PGW} - SA_{AW})(\Theta_{WW} - \Theta_{AW})}{SA_{WW} - SA_{AW}}}. \quad (1)$$

The Conservative Temperature and Absolute Salinity values for each of the three end-member water masses are summarized in Table 1, along with the corresponding potential temperature $\theta$ and practical salinity:

- for AW, these were obtained from the hydrographic properties at depth in the fjord, which are fairly homogeneous below 500 m (Fig. 2 and red in Fig. 3);
- for WW, they were inferred from the hydrographic profiles (Fig. 2) by linear extrapolation onto the freezing line; and
- for PGW, the temperature is a theoretical end member that represents the latent heat needed to melt the ice from PG with AW (Jenkins 1999). Straneo et al. (2012) define it as

$$\theta_{PGW} = \theta_f - \frac{L}{c_w} - \frac{c_i}{c_w}(\theta_f - \theta_{ice}), \quad (2)$$

where $\theta_f = -2.37$°C is fixed as the freezing temperature at the grounding line (Jackson and Straneo 2016), $L$ = 333.55 kJ kg$^{-1}$ is the latent heat of fusion, $c_w$ = 3.98 kJ kg$^{-1}$ K$^{-1}$ is the specific heat capacity of water, $c_i$ = 2.05 kJ kg$^{-1}$ K$^{-1}$ is the heat capacity of ice, and $\theta_{ice}$ = −20°C. The uncertainty of the value is mostly caused by the range of depth of the grounding line of 500 ± 100 m (Rignot and Steffen 2008). The corresponding Conservative Temperature is obtained from the "Gade-like relationship" of McDougall et al. (2014):

$$SA\frac{\delta\Theta}{\delta SA}\bigg|_{p=0\text{dbar}} = \Theta - \frac{h_{ice}}{c_w}, \quad (3)$$

where $h_{ice}$ is the enthalpy of the ice with temperature $\theta_{ice}$. McDougall et al. (2014) showed that the uncertainty of $\Theta_{PGW}$ is only 0.15% when working with this simple equation for the surface instead of the more complex equation for a pressure of 500 dbar (corresponding to the grounding line).

Varying the properties of the AW and WW end members within the ranges found in the study area (Table 1) results in up to 30% difference in the meltwater content. The meltwater content is increased if AW and/or WW are lighter (fresher and/or warmer) and decreased if they are denser (saltier and/or colder) than the reference values shown in Table 1. The meltwater content is not sensitive to changes in the PGW temperature.

The same method was applied to the casts 26 to 46 (Fig. 1) where the oxygen concentration is available. The AW oxygen end-member value (Table 1) was obtained from the hydrographic properties in the fjord as for the temperature and salinity (Fig. 4). The PGW value of 27 ml l$^{-1}$ is given by, for example, Johnson et al. (2011); its

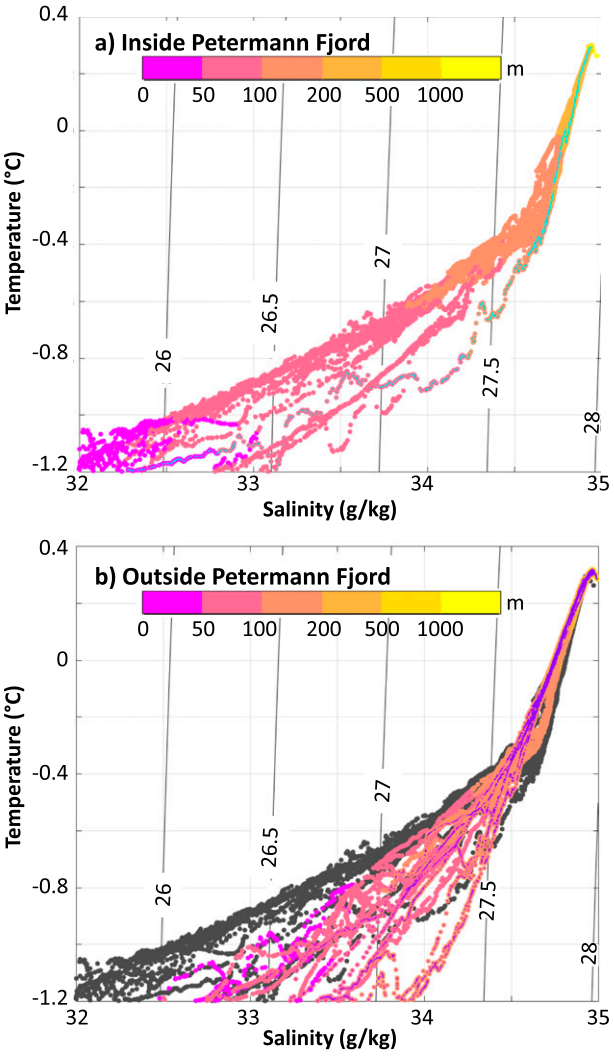


FIG. 2. Conservative Temperature–Absolute Salinity diagram, colored by depth on a logarithmic scale for all casts (a) inside the fjord and (b) outside the fjord [gray dots are the same points as (a) for comparison]. Colored dots with a cyan center in (a) indicate cast 30 (closest to glacier terminus) while those with a dark purple center in (b) indicate the casts by the Canadian coast.

uncertainty was estimated by fitting the Gade line to the *T*–O2 and *S*–O2 diagrams (Fig. 4). The WW value was inferred by linear extrapolation using the temperature and salinity WW values and the *T*–O2 and *S*–O2 diagrams (Fig. 4). For these casts, the meltwater content was calculated using the three end-member method of Eq. (1) three times:

- with the temperature and salinity (as for all the other casts, black lines in Fig. 5);
- with the temperature and oxygen concentration (blue lines in Fig. 5); and
- with the salinity and oxygen concentration (orange lines in Fig. 5).

An agreement between the three calculations indicates that our estimates are robust, while divergence—as is often seen in the top 100 m of our casts (Fig. 5)—indicates a degenerescence of the three end-member method, for example, due to the presence of another water mass or a surface flux. While below about 100 m, water mass properties are set purely by mixing between AW, PGW, and WW, properties higher in the water column are affected also by surface processes such as heating and cooling and sea ice formation and melt.

Geostrophic velocities were calculated as in Johnson et al. (2011). The thermal wind equation was used to give vertical shear relative to the bottom, and a uniform, small (barotropic), compensating velocity was added to ensure a net zero volume flux across the measured section. This is a reasonable assumption in fjords with little runoff, such as Petermann (Jackson and Straneo 2016).

## 3. Meltwater detection

We first assess whether any meltwater can be detected inside and outside Petermann Fjord using the three end-member mixing method of Jenkins (1999) for the melting of glacial ice into a stratified water column [Eq. (1)]. Figure 2 shows temperature–salinity (*T*–*S*) plots of the casts inside and outside the fjord. Inside the fjord (Fig. 2a), all casts show similar characteristics below 50-m depth; the points are arranged along two approximately straight lines in *T*–*S* space, which intersect around 150-m depth. Cast 30, taken at a location where a part of the ice tongue broke off at the beginning of the cruise, is the only one not having a clear straight line between 50 and 150 m but rather a series of wiggles (dots with a cyan center in Fig. 2a), indicative of active mixing processes and interleaving, possibly an adjustment to the removal of the ice. For all casts inside the fjord, the intersection between the two lines occurs between −0.4° and −0.3°C and around 34.6 g kg$^{-1}$ (Fig. 2a). Outside the fjord most casts have *T*–*S* properties similar to those inside the fjord (Fig. 2b).

Figure 3 shows one of the profiles from inside the fjord along with the AW–WW and AW–PGW (also known as the Gade line, from Gade 1979) mixing lines. As can be seen, the deep-water masses have points on the Gade line indicating that the water is made of a "pure" mixture between AW and basal meltwater only. This is a feature common to all the casts inside the fjord (Fig. 2a). All the casts depart from the Gade line higher in the water column, although the properties of the corresponding departure point or kink evolve with distance from the glacier (Fig. 2). Inside the fjord the kink point is fresher and colder. This kink is a clear break in the slope of the *T*–*S* diagram; the water below it is on the Gade

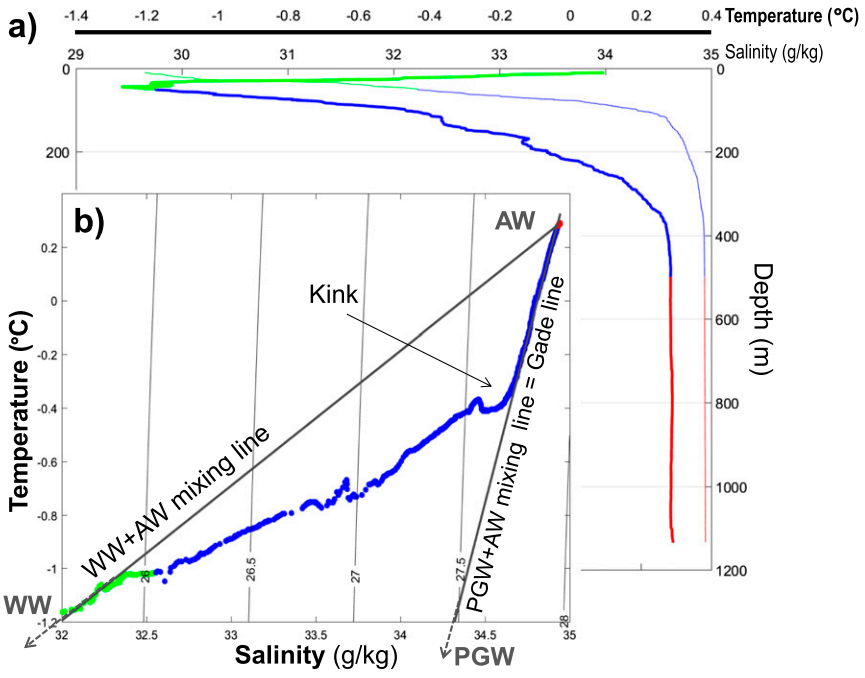


FIG. 3. Cast 13 (inside the fjord), (a) profile of Conservative Temperature (thick line) and Absolute Salinity (thin line) with depth; (b) Conservative Temperature–Absolute Salinity diagram. Thin black lines in (b) indicate the density. The terminology used throughout the paper is also illustrated in (b) (see text and Table 1 for the values of the three end members AW, WW, and PGW). For both panels, green color denotes depths from the surface to 50 m, blue indicates 50 to 500 m, and red indicates 500 m to the bottom.

line, but the water above it tends toward WW in a second straight line (Fig. 3a). This means that only two consecutive water masses mix: AW with basal meltwater and then the meltwater–AW mixture with WW. A kink in the *T*–*S* plot is seen in hydrographic data close to many marine-terminating glaciers in Greenland (Straneo et al. 2012).

The hydrographic profiles close to the coast of Ellesmere Island (Canada), on the west side of Nares Strait, are significantly different (dots with a purple center in Fig. 2b),

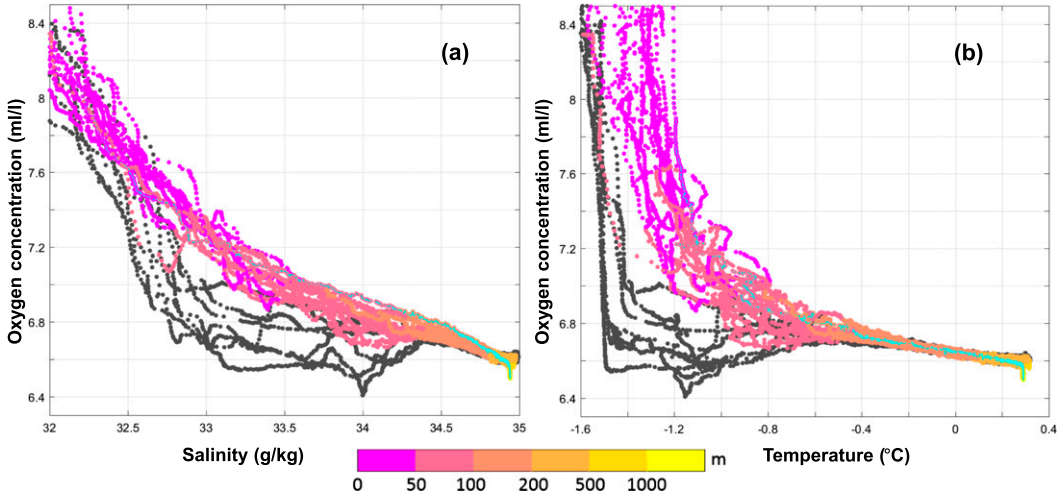


FIG. 4. (a) Oxygen concentration–Absolute Salinity and (b) oxygen concentration–Conservative Temperature diagrams for casts 26 to 46 (after 20 Aug 2015). Colors indicate the depth, using a logarithmic scale. Gray dots are casts in the Arctic inflow along the coast of Ellesmere Island (see text). Dots with a cyan center indicate cast 30.

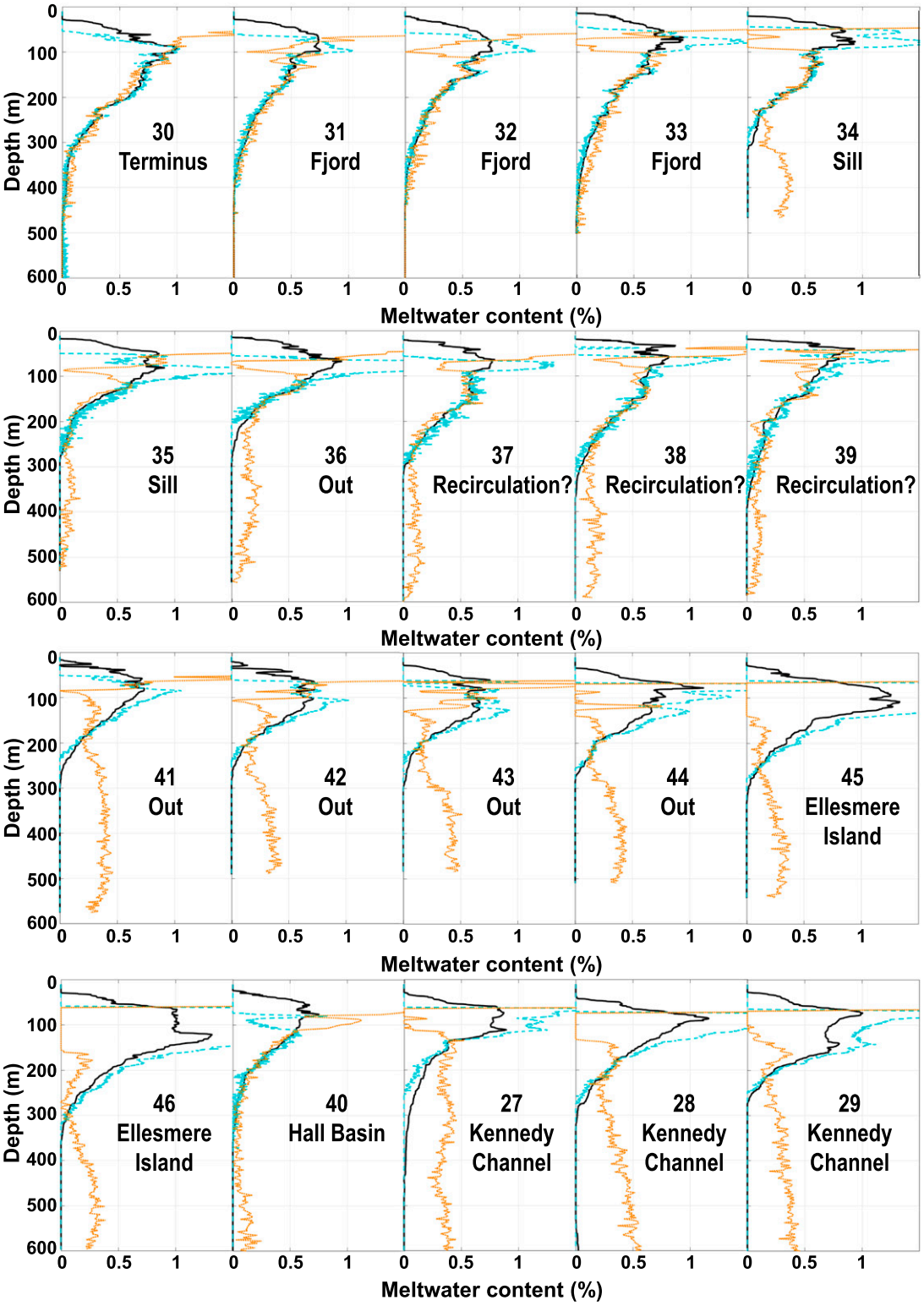


FIG. 5. Profiles of meltwater content with depth for casts 27 to 46 (see location in Fig. 1), ordered according to their distance from the terminus. Black line is obtained using only temperature and salinity, blue dashed line is obtained using temperature and oxygen concentration, and orange line is obtained using salinity and oxygen concentration.

aligning mostly along one line of slope $-1.6°C\,g^{-1}\,kg^{-1}$ and not exhibiting any clear break in slope; these correspond to the water flowing through Nares Strait from the Arctic (e.g., Münchow and Melling 2008; Johnson et al. 2011). Absolute Salinity–oxygen concentration and Conservative Temperature–oxygen concentration diagrams show that these casts in the Arctic outflow are made up of different water masses than the other casts (Fig. 4, gray dots are the Arctic inflow). Note that Fig. 4 shows only the oxygen concentration from cast 26 onward, since a pump failure rendered all oxygen measurements before that unreliable. The Arctic outflow casts have low-salinity, low-oxygen waters from 50- to 200-m depth (Fig. 4a) and are the coldest and least oxygenated that we measured during the whole expedition (Fig. 4b; as low as $-1.5°C$ for $6.55\,ml\,l^{-1}$). For all the other casts and for salinities greater than $34\,g\,kg^{-1}$ (deeper than 100 m), the salinity–oxygen diagram follows a slope that intercepts the oxygen axis ($S = 0$) at around $27\,ml\,l^{-1}$ (colored dots in Fig. 4a). This is consistent with mixing between AW and the freshwater that results from the melting of the ice shelf, where the trapped air bubbles dissolve into the mixture (Jenkins 1999).

The meltwater content obtained using Eq. (1) differs for casts inside and outside of the fjord (Fig. 5). Since the surface waters are affected by water mass transformation such as cooling, precipitation, and sea ice processes (as shown by the large differences between the three calculations; Fig. 5), we neglect the region above 100 m from our analysis. The maximum value inside the fjord is about 1% (Fig. 5, casts 30 to 33), which is consistent with the meltwater content obtained by Johnson et al. (2011) in Petermann Fjord and in agreement with the theoretical maximum value of 1% per degree above freezing of AW found by Jenkins (1999). The values found in the fjord are consistent throughout the three calculations (temperature and salinity, black line; temperature and oxygen, blue line; and temperature and salinity, orange line; Fig. 5) and are hence robust, which indicates that the assumption of mixing between the three water masses with the specified temperature, salinity, and oxygen concentrations is valid. Straneo et al. (2013) suggest that the poorly understood, small-scale processes that control the rate of heat delivery from the ocean to the floating ice tongue might be the factor limiting the meltwater content.

Outside the fjord, the maximum meltwater content is smaller (of order 0.5%, e.g., cast 36, Fig. 5). The thickness of the meltwater layer decreases with the distance from the fjord. One possibility is that as the meltwater-laden outflow moves away from the glacier it gradually mixes with lighter, ambient water. Another possibility is that some of the meltwater escapes in a narrow coastal current that was not captured by our survey since no casts were taken sufficiently close to the coast (the Rossby radius, and hence the expected width of such a current, is estimated to be approximately 4.5 km based on a 100-m-thick meltwater layer).

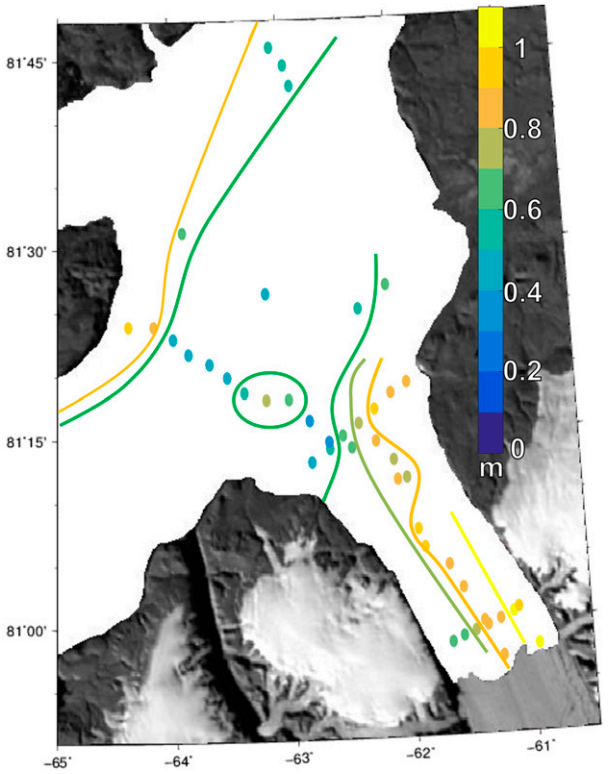


FIG. 6. Map of the meltwater content integrated between 100 and 500 m (i.e., equivalent freshwater depth), along with approximate contours.

Integrating the meltwater content obtained with the temperature and salinity for all casts from 100 to 500 m (maximum depth of the sill) provides the equivalent freshwater height of this meltwater. This amount varies substantially inside the fjord (Fig. 6) with the largest values found on the northeastern side and closest to the terminus, consistent with the local, anticlockwise circulation deduced by Johnson et al. (2011; the geostrophic circulation during our survey is discussed further in section 4). Varying the properties of the AW and WW end members within the ranges found in the study area (Table 1) results in an up to 30% difference in the meltwater content. These differences are consistent throughout our study area and do not change the main results about the circulation and meltwater flux. Outside the fjord, the meltwater freshwater height decreases with distance from the mouth of Petermann Fjord. However, the casts close to Ellesmere Island, in the Arctic outflow through Nares Strait, have larger meltwater freshwater

height: just under 1 m, compared with 0.45 m in central Hall Basin and 1.2 m close to the glacier terminus inside the fjord (Fig. 6). This is likely due to the presence of a fourth water mass (as discussed above), as can be seen in Fig. 5 where the three lines for the calculations based on the three end-member equation diverge (Fig. 5, casts 45 and 46). It could also be an artifact of the sea ice–rich waters coming from the Arctic Ocean, whose signature on the *T*–*S* diagram match those of glacial meltwater (Moore and Wallace 1988).

## 4. Meltwater circulation

Our measurements included two synoptic sections, one at the glacier's terminus and for the first time one at the sill, allowing us to compute the geostrophic velocity through these sections. The distance between the casts at the sill is less than 3 km and less than 2 km at the terminus, so that we can resolve the Rossby radius of deformation of about 4.5 km for a 100-m-thick meltwater layer. Note also that the deformation radius is about 4 times smaller than the fjord width at the sill; it is possible that significant amounts of meltwater leave the fjord in a coastally trapped boundary current. Because of logistical constraints, we lack temperature and salinity values for the top 10 m of the water column as well as within 5 km of each side of the fjord.

At the glacier's terminus, the isopycnals rise toward the southwestern side (Fig. 7a, toward the right), associated with an outwardly directed geostrophic flow at the surface that weakens and reverses direction at depth. Below 200 m, this water flowing into the cavity under the ice shelf (Fig. 7b, negative values) contains hardly any meltwater (Fig. 7c); this is the modified Atlantic Water, which ventilates the fjord (Johnson et al. 2011). On the northeastern side of the fjord, in contrast, between about 100 and 280 m, water with a large concentration of glacial meltwater is leaving the underice cavity (left of Figs. 7b,c). This is in agreement with the larger, integrated meltwater content found on the northeastern side compared with the southwestern side of the terminus section in Fig. 6.

Everywhere on the terminus section, there is a core of meltwater-rich waters between 150- and 200-m depth (Fig. 7c). This depth does not seem to vary with the draft of the ice shelf, which is locally reduced to about 60 m by underice channels running parallel to the ice shelf over its entire length (gray line in Fig. 7c). The relatively uniform distribution of meltwater suggests that melting is not occurring in the crests of the underice channels but rather at greater depths and that horizontal mixing processes are acting to distribute basal meltwater once it emerges at depth from under the ice.

The geostrophic velocity field suggests a second outflow of meltwater above 200 m on the southwest side of the terminus section. It is possible that this is associated with the basal channel located at approximately 7 km from the start of the section. In a modeling study of the ocean circulation under an idealized Petermann ice tongue, Millgate et al. (2013) showed that we might expect meltwater outflows to exit the underice cavity on the northeast side of each channel.

Close to the surface and to the fjord walls we do not expect the flow to be in geostrophic balance due to the importance of friction and wind forcing. The velocity field in the upper 100 m also seems to feature eddies (Fig. 7b), possibly associated with the surface runoff that we observed, also observed in 2009 (Johnson et al. 2011) and via remote sensing (e.g., Nick et al. 2012). The strong velocities visible in this snapshot may hence not be indicative of the time-mean flow.

There is some spatial variability in the integrated meltwater content at casts in the center of the fjord between the terminus and the sill (Fig. 6). At the sill, however, the integrated meltwater content between 100 and 500 m decreases monotonically from the northeast side of the fjord. Although we have no measurements close to the fjord walls, the strongest integrated meltwater content on the northeast side of the sill suggests that the basal meltwater is exiting the fjord as a baroclinic flow on the northeastern side, keeping the coast to its right. This is in accordance with large-scale rotating fluid dynamics.

At the sill, the hydrographic properties (Fig. 8a) and geostrophic velocities (Fig. 8b) again suggest an inflow of Atlantic Water to the fjord at depths below about 150 m. This inflow particularly seem to occur on the southwest side of the fjord where no meltwater is observed in this depth range (Fig. 8), but the three end-member method degenerates there because of the comparatively high oxygen concentrations of the more recently ventilated inflowing waters (Fig. 5, cast 34). There is a meltwater-rich outflow on the northeastern side of the sill section (likely also extending northeast of our section to the coast itself) in the approximate depth range 75 to 250 m, with a second outflow through a narrow band higher in the water column over the southwestern half of the section, where there are higher peaks of meltwater concentrations (up to 1%).

We can infer from Fig. 6 that, once outside the fjord, the meltwater from the northeastern side of the sill first turns north and follows the Greenland coast. This outflow seems to extend to the middle of Hall Basin, where our only cast (40) contains large and robust meltwater concentrations between 120- and 300-m depth (Fig. 5). It also seems feasible that basal meltwater leaving the

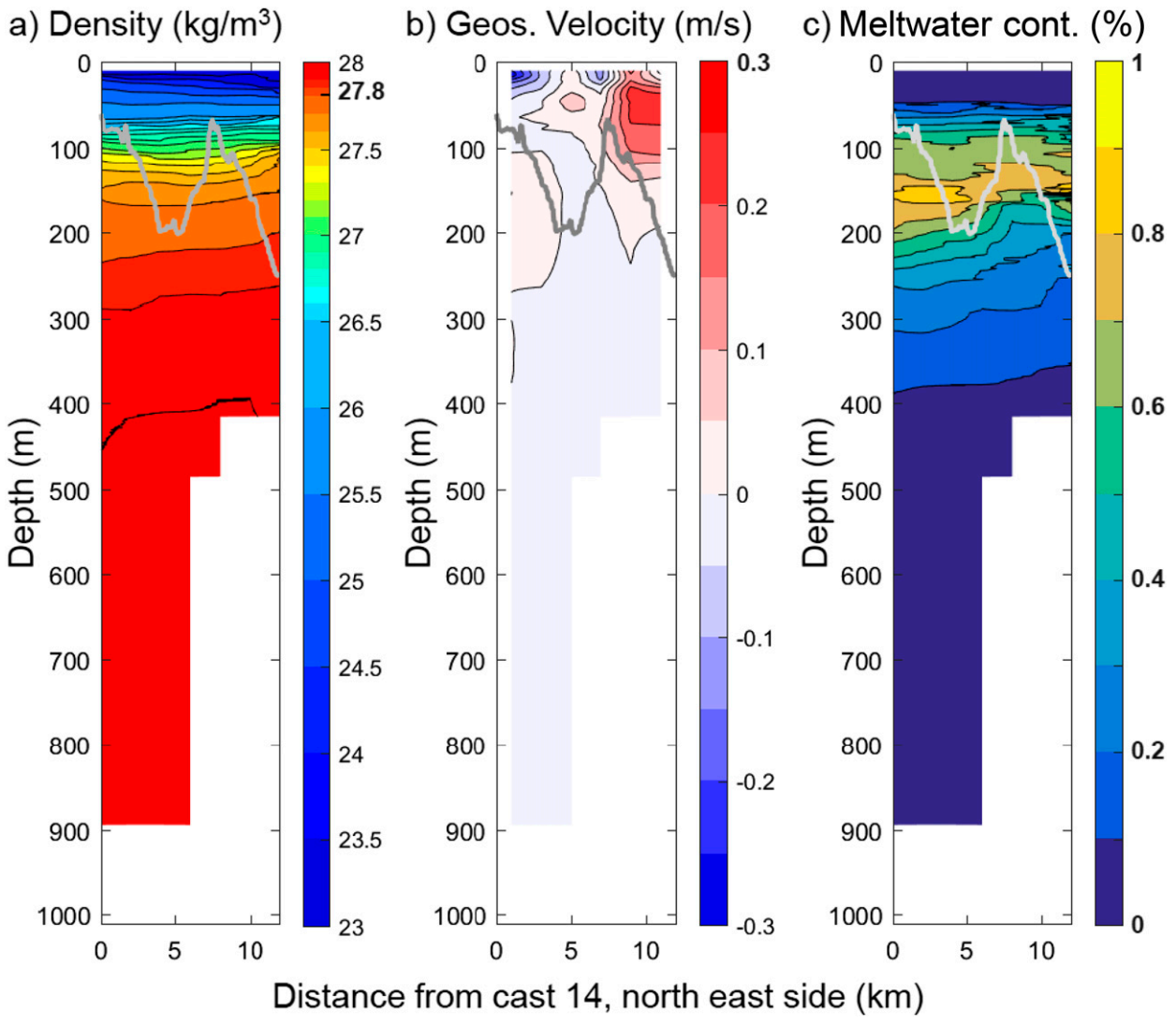


FIG. 7. Cross section close to the glacier's terminus, looking into the fjord toward the glacier (casts 14 to 8). Contours with depth and distance from the north east side of (a) density, (b) geostrophic velocity (vertical shear relative to the sea floor + uniform barotropic correction), and (c) meltwater content. Gray line in each panel is the draft of the ice shelf (after Münchow et al. 2014). Positive velocities are directed out of the fjord.

fjord closer to the center of the sill either turns right or recirculates in the small, cyclonic gyre detected by Johnson et al. (2011) before reentering the fjord on the southwestern side. The latter is consistent with the robust comparatively large meltwater concentrations encountered between 100 and 300 m in casts 37 to 39 (Fig. 5 and circled area in Fig. 6).

In Hall Basin, the flow is generally southward and strongest along the coast of Ellesmere Island, with a northward component along the coast of Greenland (Münchow and Melling 2008). Hence, for the casts that have a large, meltwater content that does not come solely from Petermann Fjord (see casts 45 and 46 in Fig. 5 and Fig. 6 by Ellemere Island), the additional freshwater source is probably located upstream in the Arctic. It could also come from Ellesmere Island itself, although all glaciers in the vicinity of Hall Basin terminate on land and hence could not feed these casts with basal meltwater. Alternatively, this seemingly strong glacial meltwater content close to Ellesmere Island could be an artifact caused by sea ice melt farther upstream (Moore and Wallace 1988). No section was performed this year across Kennedy Channel to track the water leaving Hall Basin toward the south. However, it should be noted that in our analysis, no cast was found that contained zero meltwater (even when using the densest values of the end members); hence, we can assume that some meltwater from Petermann

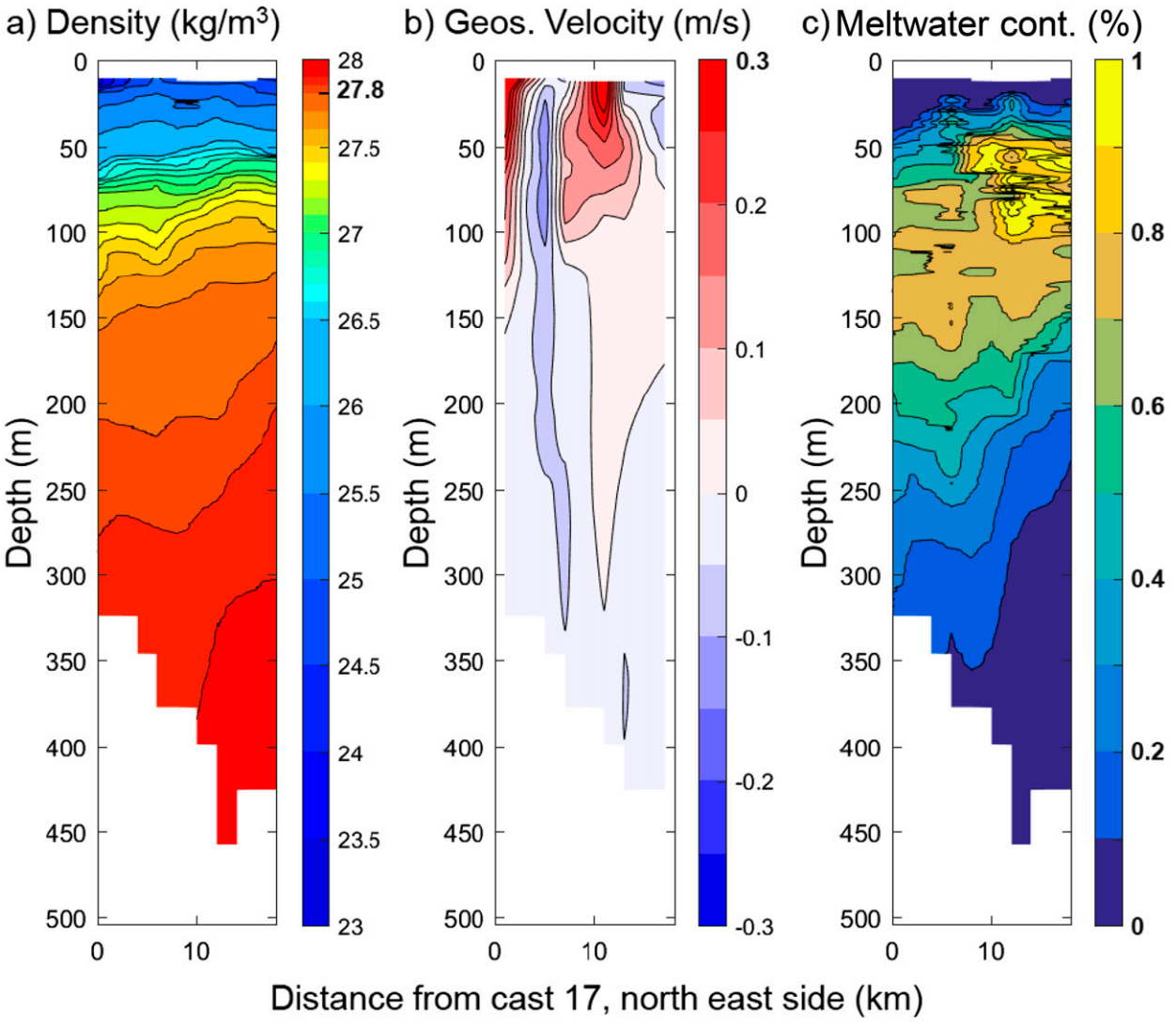


FIG. 8. As in Fig. 7, but at the sill, looking into the fjord toward the glacier (casts 17 to 23).

must leave Hall Basin through the mostly southward flow.

## 5. Discussion and conclusions

In the present paper we have observed for the first time the path of the meltwater from the Petermann floating ice tongue. Geostrophic velocities and meltwater distributions suggest an anticlockwise circulation, with inflow of Atlantic Water toward the glacier below about 200 m on the southwestern side of the fjord and outflow of meltwater-enriched water higher in the water column, particularly on the northeastern side. This is consistent with rotational fluid dynamics, for which the flow is along depth contours with a coast or shallow water on its right in the Northern Hemisphere. A similar pattern was inferred in Johnson et al. (2011) from the meltwater distribution and geostrophic velocities along a single section but is here complemented by quantitative estimates of the basal meltwater concentration spanning a large portion of the (now larger) fjord, including the first hydrographic section conducted at the sill. Inside the fjord the meltwater layer behaves like a subsurface but relatively buoyant baroclinic flow and travels from the terminus to the sill with the coast on its right (Fig. 6). Outside the fjord, the majority of the meltwater appears to follow the coastline toward the Arctic, but we also identified a potential gyre that could reinject some meltwater into the fjord via the southwestern side of the sill. Since the Rossby radius is about 4.5 km and most of the freshwater is likely contained in a boundary current within a couple of kilometers of the

coast, future sections should include casts closer to the coast.

PG was extensively studied after the 2007 and 2009 hydrographic surveys by Johnson et al. (2011). Petermann then calved dramatically in 2010 and 2012. In 2009, the Petermann ice shelf was approximately 70 km long by 16.6 km wide (Johnson et al. 2011). The thickness of the ice tongue decreased from 600 m at the grounding line to about 50 m at the terminus (Rignot and Steffen 2008). The glacier was flowing at about 1130 m $yr^{-1}$ (Johnson et al. 2011), resulting in a net freshwater flux F out of the fjord due to glacial melting between the terminus and the grounding line of 0.32 mSv (1 Sv $\equiv 10^6$ $m^3$ $s^{-1}$).

The 2015 values are given by Münchow et al. (2014): the length of Petermann ice tongue was only approximately 48 km for an unchanged width, the thickness of the ice tongue was unchanged at the grounding line but around 200 m at the terminus, and the glacier speed at the grounding line had accelerated to 1250 ± 90 m $yr^{-1}$. This results in a net glacial meltwater flux out of the fjord of 0.26 mSv. Although the glacier now flows faster, it thins by a smaller amount before reaching its calving front (400 m compared to 550 m in 2009), which results in a similar flux $F$, considering the uncertainties on the glaciological measurements.

Following Johnson et al. (2011), we compute the heat flux from the ocean $Q$ needed to melt ice at this rate $F$:

$$Q = \rho_i F(L + c_i \Delta\Theta), \tag{4}$$

where $\rho_i = 917\,\mathrm{kg\,m^{-3}}$ is the mean density of ice, $L = 333.55\,\mathrm{kJ\,kg^{-1}}$ is the latent heat of fusion, $c_i = 2.05\,\mathrm{kJ\,kg^{-1}\,K^{-1}}$ is the specific heat capacity of ice, and $\Delta\Theta = \Theta_f - \Theta_{\mathrm{ice}}$ is the difference between the fixed freezing temperature, chosen as that at the grounding line (Jackson and Straneo 2016) and the temperature of ice (taken as −20°C). In 2009, $Q = 1.1 \times 10^{11}$ W; in 2015, this flux is $0.88 \times 10^{11}$ W. Assuming that the ice shelf melting occurs entirely due to $Q$ (i.e., neglecting any surface melting), and over the whole area of the ice tongue, an average heat flux of 97 W $m^{-2}$ was required in 2009 and of 111 W $^{-2}$ in 2015 (i.e., a 15% increase).

Although the geostrophic velocity field represents a snapshot and does not span the entire width of the fjord, we calculate a first-order estimate of the ocean heat flux in the fjord using the geostrophic velocities in Figs. 7 and 8. The geostrophic heat flux $Q_g$ (Johnson et al. 2011) is

$$Q_g = \int_A \rho_w c_w (\Theta - \Theta_f) u_g \, dA, \tag{5}$$

where $A$ is the area of the section, $\rho_w = 1027\,\mathrm{kg\,m^{-3}}$ is a reference density of water, $c_w = 3.98\,\mathrm{kJ\,kg^{-1}\,K^{-1}}$ is the specific heat capacity of water, $u_g$ is the along-fjord component of geostrophic velocity, and $\Theta_f$ is the freezing temperature at the grounding line. Using the geostrophic velocity field in Fig. 8b, we find a net heat flux during the 2015 survey of $Q_g = (5.0 \pm 0.5) \times 10^{11}$ W crossing our measured section at the sill (entering the fjord), of which about $(2.5 \pm 0.5) \times 10^{11}$ W is below 100 m and continues across the terminus section (and hence into the subice shelf cavity). The uncertainty values given here are based on different choices of interpolation and reference level when estimating the geostrophic velocities and are likely underestimates of the real uncertainty in the heat flux given that our snapshot section does not span the entire fjord width and that the flow may not be geostrophic. Nevertheless, as in 2009, there is ample heat coming into the fjord to accomplish the observed melting of Petermann ice shelf ($Q_g > Q$). Excess heat may be lost to the atmosphere, to sea ice, or to the vertical calving front.

The geostrophic freshwater flux $F_g$ is

$$F_g = \int_A (1 - \mathrm{SA}/\mathrm{SA_{AW}}) u_g \, dA. \tag{6}$$

At the terminus, the flux $F_g$ across our measured section, directed away from the ice, is about 3.2 ± 0.3 mSv, of which 2.5 ± 0.3 mSv is below 100 m. Again, the 10% uncertainty quoted here comes from the uncertainty of $u_g$. At the sill, the total freshwater flux is larger (about double), of which 2.0 ± 0.2 mSv is below 100 m. These numbers are an order of magnitude larger than the subglacial melt $F$ inferred from the ice discharge because of the large number of other freshwater sources, including terrestrial runoff and sea ice melt. Note also that $F_g$ is a summer snapshot in a fjord with a strong seasonal cycle (Rignot and Kanagaratnam 2006), whereas $F$ is the annual average. Only from long-term, year-round observations could we properly conclude on their relative magnitudes.

We can estimate the flux of glacial meltwater arising only due to the oceanic melting of the ice shelf by integrating the meltwater concentration multiplied by the geostrophic velocity over each section, that is,

$$F_{\mathrm{melt}} = \int_A \mathrm{melt.content} \times u_g \, dA. \tag{7}$$

The net meltwater flux crossing the terminus section is 0.28 ± 0.03 mSv and that crossing the sill section is 0.34 ± 0.03 mSv. These numbers are close to the estimate of subglacial melt inferred from ice discharge $F$, despite the fact that they do not cover the entire fjord cross section. In particular, we lack measurements close to the wall

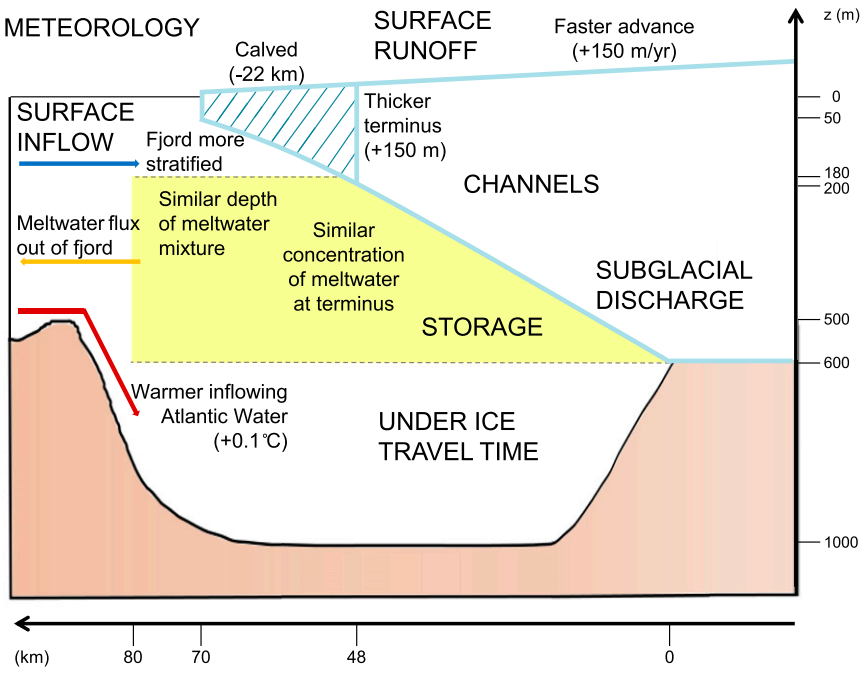


FIG. 9. Schematic of what has changed in Petermann Fjord since the study of Johnson et al. (2011). Capital letters indicate phenomena that probably have an impact on the dynamics of Petermann Fjord but whose magnitude is unknown in our study.

where a large amount of this geostrophic flow is likely to lay.

Johnson et al. (2011) hypothesized that the presence of relatively buoyant, cold WW beneath the ice shelf in 2009 was forcing the rising plume of melt-influenced water to detach from the bottom of the ice shelf, preventing basal melting from occurring once the base of the ice shelf rose above the base of the WW layer at approximately 150-m depth. Since the 2009 survey, the ice tongue has retreated by more than 20 km. Since the portion of the ice shelf that calved in 2010 and 2012 had a draft less than 100 m over much of its length, its base was in the portion of the water column occupied by WW, and it was therefore likely not melting much (Johnson et al. 2011), which could explain why the meltwater concentration has not significantly changed between 2009 and 2015. Also, despite the fact that the inflowing Atlantic Water is now 0.28°C (Table 1) and hence warmer by about 0.1°C compared to 2009 (0.19°C), we might expect that the glacial meltwater export has not changed much, since in both the 2009 and 2015 surveys we saw that the availability of ocean heat did not seem to be the factor limiting the melt rate of the ice shelf.

The thickness of Petermann ice shelf at its terminus in 2015 was about 200 m, and hence WW can no longer be expected to insulate the ice from melting by the comparatively warm Atlantic Water below (except, perhaps, in the crests of the basal channels, which now extend all the way to the terminus). We might therefore expect the ice shelf to be more sensitive to changes in ocean temperature in the future. To predict future melt rates we will need to advance our understanding of ice–ocean interactions in marine-terminating glaciers, which remains plagued by unknowns. For example we do not know what controls the stratification in the fjord and the properties of WW. Is it the atmospheric forcing, the inflow of surface waters from the Arctic, the surface runoff from the ice shelf, or a combination of all three? We also do not know the details of the circulation in the underice shelf cavity, the role of underice topography in focusing the flow, or the small-scale processes at the ice–ocean interface where melting takes place. The amount of glacial surface meltwater discharged from the base of the glacier at the grounding line is also unknown. This cannot be detected with the three end-member mixture equation since it is already liquid when it mixes with AW. These unknown processes are summarized in Fig. 9, where we also highlight the changes between 2009 and 2015.

An important observation that we lack is an estimate of the variability of the meltwater discharge and pathways. Repeat sections but also year-round and longer-term monitoring are key to assessing this and also to understanding the relationship between the properties and fate of the meltwater, the stratification in the fjord, and the geometry of the glacier. Two types of sensors

have been deployed during the Petermann 2015 expedition to try and fill this gap in our understanding of ice–ocean interactions in Petermann Fjord. Conductivity–temperature sensors are moored under the ice shelf (Münchow et al. 2016), while Long Term Underwater Sensing (LoTUS) temperature buoys (www.lotussensing.com) are anchored on the bottom of the fjord near the sill and the terminus. Both systems are already sending back data and should lead to an estimate of the variability of the ocean in Petermann Fjord on daily to yearly time scales. Continued, long-term monitoring of Greenland's marine-terminating glaciers is needed to understand their melting and to track their meltwater. This is essential if climate models are to include a reliable, interactive ice sheet component and make accurate projections of Greenland melt, together with its impact on global ocean circulation and sea level rise (Flato et al. 2013).

*Acknowledgments.* CH is supported by a VINNOVA Marie Curie research fellowship between the University of Gothenburg and the University of Oxford (2015-01487). AW is supported by VINNOVA fellowships 2010-485 and 2013-5273. The authors thank the University of Gothenburg for funding the oceanography work of the cruise, the Swedish Research Council for the equipment, and the Swedish Polar Secretariat for ship time. We are also grateful to the Sven Lovén Centre for technical assistance and to the crew and staff onboard I/B *Oden*. We thank the two anonymous reviewers whose comments notably improved the quality of this manuscript.

## REFERENCES

Aagaard, K., L. K. Coachman, and E. Carmack, 1981: On the halocline of the Arctic Ocean. *Deep-Sea Res.*, **28**, 529–545, doi:10.1016/0198-0149(81)90115-1.

Bamber, J., M. van den Broeke, J. Ettema, J. Lenaerts, and E. Rignot, 2012: Recent large increases in freshwater fluxes from Greenland into the North Atlantic. *Geophys. Res. Lett.*, **39**, L19501, doi:10.1029/2012GL052552.

Coachman, L. K., and K. Aagaard, 1974: Physical oceanography of arctic and subarctic seas. *Marine Geology and Oceanography of the Arctic Seas*, Y. Herman, Ed., Springer-Verlag, 1–72.

Enderlin, E. M., and I. M. Howat, 2013: Submarine melt rate estimates for floating termini of Greenland outlet glaciers (2000-2010). *J. Glaciol.*, **59**, 67–75, doi:10.3189/2013JoG12J049.

Falkner, K. K., and Coauthors, 2011: Context for the recent massive Petermann Glacier calving event. *Eos, Trans. Amer. Geophys. Union*, **92**, 117–118, doi:10.1029/2011EO140001.

Flato, G., and Coauthors, 2013: Evaluation of climate models. *Climate Change 2013: The Physical Science Basis*, T. F. Stocker et al., Eds., Cambridge University Press, 741–866.

Gade, H. G., 1979: Melting of ice in sea water: A primitive model with application to the Antarctic ice shelf and icebergs. *J. Phys. Oceanogr.*, **9**, 189–198, doi:10.1175/1520-0485(1979)009<0189:MOIISW>2.0.CO;2.

Jackson, R. H., and F. Straneo, 2016: Heat, salt, and freshwater budgets for a glacial fjord in Greenland. *J. Phys. Oceanogr.*, **46**, 2735–2768, doi:10.1175/JPO-D-15-0134.1.

Jacobs, S. S., A. Jenkins, C. F. Giulivi, and P. Dutrieux, 2011: Stronger ocean circulation and increased melting under Pine Island Glacier ice shelf. *Nat. Geosci.*, **4**, 519–523, doi:10.1038/ngeo1188.

Jakobsson, M., and Coauthors, 2012: The International Bathymetric Chart of the Arctic Ocean (IBCAO) version 3.0. *Geophys. Res. Lett.*, **39**, L12609, doi:10.1029/2012GL052219.

Jenkins, A., 1999: The impact of melting ice on ocean waters. *J. Phys. Oceanogr.*, **29**, 2370–2381, doi:10.1175/1520-0485(1999)029<2370:TIOMIO>2.0.CO;2.

Johnson, H. L., A. Münchow, K. K. Falkner, and H. Melling, 2011: Ocean circulation and properties in Petermann Fjord, Greenland. *J. Geophys. Res.*, **116**, C01003, doi:10.1029/2010JC006519.

Khan, S. A., and Coauthors, 2014: Sustained mass loss of the northeast Greenland ice sheet triggered by regional warming. *Nat. Climate Change*, **4**, 292–299, doi:10.1038/nclimate2161.

McDougall, T. J., and P. M. Barker, 2011: Getting started with TEOS-10 and the Gibbs Seawater (GSW) oceanographic toolbox. SCOR/IAPSO WG127, 28 pp. [Available online at www.teos-10.org/pubs/Getting_Started.pdf.]

——, ——, R. Feistel, and B. K. Galton-Fenzi, 2014: Melting of ice and sea ice into seawater and frazil ice formation. *J. Phys. Oceanogr.*, **44**, 1751–1775, doi:10.1175/JPO-D-13-0253.1.

Millgate, T., P. R. Holland, A. Jenkins, and H. L. Johnson, 2013: The effect of basal channels on oceanic ice-shelf melting. *J. Geophys. Res. Oceans*, **118**, 6951–6964, doi:10.1002/2013JC009402.

Moore, R. M., and D. W. R. Wallace, 1988: A relationship between heat transfer to sea ice and temperature–salinity properties of Arctic Ocean waters. *J. Geophys. Res.*, **93**, 565–571, doi:10.1029/JC093iC01p00565.

Münchow, A., and H. Melling, 2008: Ocean current observations from Nares Strait to the west of Greenland: Interannual to tidal variability and forcing. *J. Mar. Res.*, **66**, 801–833, doi:10.1357/002224008788064612.

——, L. Padman, and H. A. Fricker, 2014: Interannual changes of the floating ice shelf of Petermann Gletscher, north Greenland, from 2000 to 2012. *J. Glaciol.*, **60**, 489–499, doi:10.3189/2014JoG13J135.

——, ——, P. Washam, and K. W. Nicholls, 2016: The ice shelf of Petermann Glacier, north Greenland, and its connection to the Arctic and Atlantic Oceans. *Oceanography*, **29**, 84–95, doi:10.5670/oceanog.2016.101.

Nick, F., and Coauthors, 2012: The response of Petermann Glacier, Greenland, to large calving events, and its future stability in the context of atmospheric and oceanic warming. *J. Glaciol.*, **58**, 229–239, doi:10.3189/2012JoG11J242.

——, A. Vieli, M. L. Andersen, I. Joughin, A. Payne, T. L. Edwards, F. Pattyn, and R. S. W. van de Wal, 2013: Future sea-level rise from Greenland's main outlet glaciers in a warming climate. *Nature*, **497**, 235–238, doi:10.1038/nature12068.

Rignot, E., 1996: Tidal motion, ice velocity and melt rate of Petermann Gletscher, Greenland, measured from radar interferometry. *J. Glaciol.*, **42**, 476–485.

——, and P. Kanagaratnam, 2006: Changes in the velocity structure of the Greenland ice sheet. *Science*, **311**, 986–990, doi:10.1126/science.1121381.

——, and K. Steffen, 2008: Channelized bottom melting and stability of floating ice shelves. *Geophys. Res. Lett.*, **35**, L02503, doi:10.1029/2007GL031765.

Straneo, F., and Coauthors, 2012: Characteristics of ocean waters reaching Greenland's glaciers. *Ann. Glaciol.*, **53**, 202–210, doi:10.3189/2012AoG60A059.

——, and Coauthors, 2013: Challenges to understanding the dynamic response of Greenland's marine terminating glaciers to oceanic and atmospheric forcing. *Bull. Amer. Meteor. Soc.*, **94**, 1131–1144, doi:10.1175/BAMS-D-12-00100.1.

Swingedouw, D., J. Mignot, P. Braconnot, E. Mosquet, M. Kageyama, and R. Alkama, 2009: Impact of freshwater release in the North Atlantic under different climate conditions in an OAGCM. *J. Climate*, **22**, 6377–6403, doi:10.1175/2009JCLI3028.1.

Velicogna, I., T. C. Sutterley, and M. R. van den Broeke, 2014: Regional acceleration in ice mass loss from Greenland and Antarctica using grace time-variable gravity data. *Geophys. Res. Lett.*, **41**, 8130–8137, doi:10.1002/2014GL061052.

Wåhlin, A. K., X. Yuan, G. Björk, and C. Nohr, 2010: Inflow of warm circumpolar deep water in the central Amundsen shelf. *J. Phys. Oceanogr.*, **40**, 1427–1434, doi:10.1175/2010JPO4431.1.

Zwally, H. J., and Coauthors, 2011: Greenland ice sheet mass balance: Distribution of increased mass loss with climate warming; 2003–07 versus 1992–2002. *J. Glaciol.*, **57**, 88–102.